Model Compounds for Iron Proteins. Structures and Magnetic, Spectroscopic, and Redox Properties of $Fe^{III}M^{II}$ and $[Co^{III}Fe^{III}]_2O$ Complexes with (μ-Carboxylato)bis(μ-phenoxo)dimetalate and (μ-Oxo)diiron(III) Cores

Sujit K. Dutta,[†] Rüdiger Werner,[‡] Ulrich Flörke,[§] Sasankasekhar Mohanta,[†] Kausik K. Nanda,[†] Wolfgang Haase,[‡] and Kamalaksha Nag*,[†]

Department of Inorganic Chemistry, Indian Association for the Cultivation of Science, Calcutta 700 032, India, Institut für Physikalische Chemie der Technischen Hochschule, D-64287 Darmstadt, Germany, and Anorganische und Analytische Chemie der Universität Gesamthochschule Paderborn, D-33098 Paderborn, Germany

Received July 7, 1995[⊗]

A series of heterobimetallic complexes of the type $[Fe^{III}M^{II}L(\mu\text{-OAc})(OAc)(H_2O)](ClO_4)\cdot nH_2O$ (**2**−**5**) and $[\{Fe^{III}Co^{III}L(\mu\text{-OAc})(OAc)\}_2(\mu\text{-O})](ClO_4)_2\cdot 3H_2O$ (**6**) where H_2L is a tetraaminodiphenol macrocyclic ligand and M^{II} = Zn(**2**), Ni(**3**), Co(**4**), and Mn(**5**) have been synthesized and characterized. The ^1H NMR spectrum of **6** exhibits all the resonances between 1 and 12 ppm. The IR and UV−vis spectra of **2**−**5** indicate that in all the cases the metal ions have similar coordination environments. A disordered crystal structure determined for **3** reveals the presence of a (μ-acetate)bis(μ-phenoxide)−$Ni^{II}Fe^{III}$ core, in which the two metal ions have 6-fold coordination geometry and each have two amino nitrogens and two phenolate oxygens as the in-plane donors; aside from the axial bridging acetate, the sixth coordination site of nickel(II) is occupied by the unidentate acetate and that of iron(III) by a water molecule. The crystal structure determination of **6** shows that the two heterobinuclear Co^{III}-Fe^{III} units are bound by an Fe−O−Fe linkage. **6** crystallizes in the orthorhombic space group *Ibca* with a = 17.577(4) Å, b = 27.282(7) Å, c = 28.647(6) Å, and Z = 8. The two iron(III) centers in **6** are strongly antiferromagnetically coupled, $J = -100$ cm^{-1} ($H = -2JS_1\cdot S_2$), whereas the other two $S_1 = S_2 = {}^5/_2$ systems, viz. $[Fe_2^{III}(HL)_2(\mu\text{-OH})_2](ClO_4)_2$ (**1**) and the $Fe^{III}Mn^{II}$ complex (**5**), exhibit weak antiferromagnetic exchange coupling with $J = -4.5$ cm^{-1} (**1**) and -1.8 cm^{-1} (**5**). The $Fe^{III}Ni^{II}$ (**3**) and $Fe^{III}Co^{II}$ (**4**) systems, however, exhibit weak ferromagnetic behavior with $J = 1.7$ cm^{-1} (**3**) and 4.2 cm^{-1} (**4**). The iron(III) center in **2**−**5** exhibits quasi-reversible redox behavior between −0.44 and −0.48 V vs Ag/AgCl associated with reduction to iron(II). The oxidation of cobalt(II) in **4** occurs quasi-reversibly at 0.74 V, while both nickel(II) and manganese(II) in **3** and **5** undergo irreversible oxidation at 0.85 V. The electrochemical reduction of **6** leads to the generation of **4**.

Introduction

Oxo- and hydroxo-bridged diiron units are of wide occurrence in biology and perform a range of activities such as oxygen transport (hemerythrin[1]), hydroxylation of alkanes (methyl monooxygenase[2]), phosphate ester hydrolysis (purple acid phosphatases,[3] PAP's) and DNA synthesis (ribonucleotide reductase[4]). Consequently, the structural, magnetic, spectroscopic and redox properties, as also chemical reactivities of binuclear iron complexes have been the focus of intense activities.[5−11] The recognition of $Fe_2(\mu\text{-O})(\mu\text{-O}_2CR)_2$ and $Fe_2(\mu\text{-O})(\mu\text{-O}_2CR)$ cores in the active sites of some of the diiron proteins have led to the production of a few excellent structural models.[12]

The occurrence of a heterobimetallic $Fe^{III}Zn^{II}$ active site in the PAP from kidney bean[13] has evoked considerable interest because PAP's from bovine spleen and porcine uterin fluid

[†] Indian Association for the Cultivation of Science, Calcutta.
[‡] Technische Hochschule, Darmstadt.
[§] Universität Gesamthochschule Paderborn.
[⊗] Abstract published in *Advance ACS Abstracts,* March 15, 1996.

(1) (a) Holmes, M. A.; Stenkamp, R. E. *J. Mol. Biol.* **1991**, *220*, 723. (b) Sheriff, S.; Hendrickson, W. A.; Smith, J. L. *J. Mol. Biol.* **1987**, *197*, 273. (c) Shiemke, A. K.; Loehr, T. M.; Sanders-Loehr, J. *J. Am. Chem. Soc.* **1986**, *108*, 2437.
(2) (a) Rosenzweig, A. C.; Frederick, C. A.; Lippard, S. J.; Nordlund, P. *Nature* **1993**, *366*, 537. (b) Anderson, K. K.; Froland, W. A.; Lee, S.-K.; Lipscomb, J. D. *New J. Chem.* **1991**, *15*, 405. (c) Green, J.; Dalton, H. *J. Biol. Chem.* **1989**, *264*, 17698.
(3) (a) True, A. E.; Scarrow, R. C.; Randall, C. R.; Holz, R. C.; Que, L., Jr. *J. Am. Chem. Soc.* **1993**, *115*, 4246. (b) Averill, B. A.; Davis, J. C.; Burman, S.; Zirino, T.; Sanders-Loehr, J.; Loehr, T. M.; Sage, J. T.; Debrunner, P. G. *J. Am. Chem. Soc.* **1987**, *109*, 3760. (c) Antanaitis, B. C.; Aisen, P. *Adv. Inorg. Biochem.* **1983**, *5*, 111.
(4) (a) Nordlund, P.; Eklund, H. *J. Mol. Biol.* **1993**, *232*, 123. (b) Atta, M.; Nordlund, P.; Aberg, A.; Eklund, H.; Fontecave, M. *J. Biol. Chem.* **1992**, *267*, 20682.
(5) (a) Feig, A. L.; Lippard, S. J. *Chem. Rev.* **1994**, *94*, 759. (b) Lippard, S. J. *Angew. Chem., Int. Ed. Engl.* **1988**, *27*, 344.
(6) (a) Que, L., Jr. in *Bioinorganic Catalysis*; Reedijk, J., Ed.; Marcel Dekker: Amsterdam, 1993; p 347. (b) Que, L., Jr.; True, A. E. *Prog. Inorg. Chem.* **1990**, *38*, 97.
(7) Kurtz, D. M., Jr. *Chem. Rev.* **1990**, *90*, 585.
(8) Vincent, J. B.; Olivier-Lilley, G. L.; Averill, B. A. *Chem. Rev.* **1990**, *90*, 1447.
(9) Sanders-Loehr, J. In *Iron Carriers and Iron Proteins*; Loehr, T. M., Ed.; VCH Publishers: New York, 1989; p 373.
(10) Wilkins, P. C.; Wilkins, R. G. *Coord. Chem. Rev.* **1987**, *7*, 195.
(11) Murray, K. S. *Coord. Chem. Rev.* **1974**, *12*, 1.
(12) For example, see: (a) Armstrong, W. H.; Lippard, S. J. *J. Am. Chem. Soc.* **1983**, *105*, 4837. (b) Wieghardt, K.; Pohl, K.; Gebert, W. *Angew. Chem., Int. Ed. Engl.* **1983**, *22*, 727. (c) Armstrong, W. H.; Spool, A.; Papaefthymiou, G. C.; Frankel, R. B.; Lippard, S. J. *J. Am. Chem. Soc.* **1984**, *106*, 3653. (d) Chaudhuri, P.; Wieghardt, K.; Nuber, B.; Weiss, J. *Angew. Chem., Int. Ed. Engl.* **1985**, *24*, 778. (e) Turowski, P. N.; Armstrong, W. H.; Roth, M. E.; Lippard, S. J. *J. Am. Chem. Soc.* **1990**, *112*, 681. (f) Drueke, S.; Wieghardt, K.; Nuber, B.; Weiss, J.; Fleischhauer, H.-P.; Gehring, S.; Haase, W. *J. Am. Chem. Soc.* **1989**, *111*, 8622. (g) Norman, R. E.; Yan, S.; Que, L., Jr.; Backes, G.; Ling, J.; Sanders-Loehr, J.; Zhang, J. H.; O'Connor, C. J. *J. Am. Chem. Soc.* **1990**, *112*, 1554. (h) Dong, Y.; Menage, S.; Brennan, B. A.; Elgren, T. A.; Jang, H. G.; Pearce, L. L.; Que, L., Jr. *J. Am. Chem. Soc.* **1993**, *115*, 1851.

0020-1669/96/1335-2292$12.00/0

(uteroferrin) contain the $Fe_2(\mu$-O) core. Further, while one of the iron sites in the mammalian PAP's in the reduced state can be substituted by bivalent metal ions to produce $Fe^{III}M^{II}$ derivatives,[14] the Zn^{II} site in kidney bean PAP on substitution with Fe^{II} produces an enzyme that resembles mammalian PAP's under reducing conditions.[15]

In order to understand such systems, Que et al. have made comprehensive[16−19] studies on a series of heterobinuclear $Fe^{III}M^{II}$ (M = Zn,[16] Cu,[17] Ni,[18] or Mn[19]) complexes of the binucleating ligand HBPMP.[20] In these structurally similar complexes, all having a μ-phenoxo−bis(μ-carboxylate) core, the two metal centers (except for $Fe^{III}Zn^{II}$) are antiferromagnetically coupled. These studies have provided information about the ground and excited state EPR signals, zero-field splitting parameters and magnetic hyperfine coupling constants. A recent crystal structure determination of a PAP containing a dinuclear $Fe^{III}Zn^{II}$ active site[21] has helped to rationalize the postulated mechanism of phosphate ester hydrolysis by an iron(III)-coordinated hydroxide ion.[22]

In the course of our studies on magnetostructural relationships in metal complexes of the tetraaminodiphenol macrocyclic ligand H_2L we have examined several types of homo- and heterobinuclear species,[23] including the carboxylato-bridged complexes.[24] The present study is concerned with the structural characterization, electrochemical behavior and magnetic properties of the heterobinuclear complexes $[Fe^{III}M^{II}L(\mu\text{-OA})(OAc)(H_2O)](ClO_4)\cdot$solvent (M = Zn, Ni, Co, or Mn) and the heterotetranuclear complex $[\{Fe^{III}Co^{III}L(\mu\text{-OAc})(OAc)\}_2(\mu\text{-O})](ClO_4)_2\cdot 3H_2O$.

Experimental Section

All reagents and solvents were purchased from commercial sources and used as recieved. The macrocyclic ligand H_2L was prepared according to previously published procedures.[25] Elemental (C, H, and N) analyses were performed on a Perkin-Elmer 240C analyzer, while the metal analyses were carried out by standard volumetric and gravimetric methods.[26]

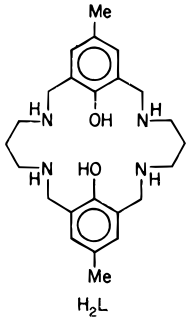

H_2L

Synthesis of Complexes. $[Fe_2^{III}(HL)_2(\mu\text{-OH})_2](ClO_4)_2$ (1). The preparation and characterization of this compound has been already reported.[27] An alternative method of synthesis is given here. To a methanol solution (20 mL) of $Fe(ClO_4)_3\cdot 6H_2O$ (0.92 g, 2 mmol) was added a solution of H_2L (0.82 g, 2 mmol) dissolved in methanol (50 mL) at room temperature with stirring. After a short while 1.3 g of NaOAc dissolved in methanol (30 mL) was added, when the color of the solution changed from deep violet to dark red. After 2 h, the red microcrystalline compound that deposited was collected by filtration, washed with methanol, and recrystallized from acetonitrile−ethanol (1:4). Yield: 0.82 g; 70%.

$[Fe^{III}Zn^{II}L(\mu\text{-OAc})(OAc)(H_2O)](ClO_4)\cdot H_2O$ (2), $[Fe^{III}Ni^{II}L(\mu\text{-OAc})(OAc)(H_2O)](ClO_4)\cdot 2H_2O$ (3), $[Fe^{III}Co^{II}L(\mu\text{-OAc})(OAc)(H_2O)](ClO_4)\cdot 2H_2O$ (4), $[Fe^{III}Mn^{II}L(\mu\text{-OAc})(OAc)(H_2O)](ClO_4)\cdot 2H_2O$ (5). All these complexes were prepared in the same way as illustrated before for **4**, which is typical of the series.

To a solution (50 mL) of **1** (0.58 g, 0.5 mmol) and NaOAc (0.33 g, 4 mmol) in acetonitrile−methanol (1:1) mixture was added 0.37 g (1 mmol) of $Co(ClO_4)_2\cdot 6H_2O$ in an atmosphere of nitrogen. The resulting blue violet solution was stirred at room temperature for 1 h and then bulk of the solvent (ca. 45 mL) was removed by flash evaporation. Addition of ice-cooled ethanol (10 mL), followed by standing at 10 °C (1 h) led to the deposition of the blue violet microcrystals of **4**. The product was collected by filtration and recrystallized from hot ethanol (0.64 g, 80%). The yield for the other compounds varied between 75−85%. The preparations of **2** and **3** were carried out in open air.

$[\{Fe^{III}Co^{III}L(\mu\text{-OAc})(OAc)\}_2(\mu\text{-O})](ClO_4)_2\cdot 3H_2O$ (6). The preparation of **4**, as described above, was initiated in ethanol (50 cm^3). To the blue violet solution an aqueous solution of NaOH (1 mL, 0.1 M) was added when the color changed to cherry red. The solution was cooled to 10 °C and slowly treated with 0.8 mL of H_2O_2 (30%) diluted with ethanol (10 mL) over a period of 30 min. The color of the solution changed to greenish brown and stirring was continued for 6 h, during which time a greenish brown microcrystalline compound deposited. After standing for an overnight period the solid deposited was collected by filtration, washed with ethanol, and air-dried. Recrystallization from acetonitrile−ethanol (1:5) afforded olive green crystals of **6** (0.11 g, 15%).

Analytical results of the compounds are given in Table S1.

Caution! Perchlorate salts of metal complexes are potentially explosive and therefore should be prepared and handled in small quantities.

Physical Methods. IR spectra were recorded on a Perkin-Elmer 783 spectrophotometers using KBr disks. Electronic spectra were obtained with Shimadzu UV 2100 and Hitachi U3400 spectrophotometers over the UV−vis and near-IR regions. Solutions were in acetonitrile and *N*,*N*′-dimethylformamide (DMF). ^{1}H NMR spectra were obtained on a Bruker AC 250 spectrometer using CD_3CN and CD_3NO_2 solutions with TMS as the internal standard.

(13) Beck, J. L.; McConachie, L. A.; Summors, A. C.; Arnold, W. N.; deJersey, J.; Zerner, B. *Biochim. Biophys. Acta* **1986**, *869*, 61.
(14) (a) Davis, J. C.; Averill, B. A. *Proc. Natl. Acad. Sci. U.S.A.* **1982**, *79*, 4623. (b) Beck, J. L.; Keough, D. T.; de Jersey, J.; Zerner, B. *Biochim. Biophys. Acta* **1984**, *791*, 357. (c) David, S. S.; Que, L., Jr. *J. Am. Chem. Soc.* **1990**, *112*, 6455. (d) Holz, R. C.; que, L., Jr.; Ming, L.-J. *J. Am. Chem. Soc.* **1992**, *114*, 4434.
(15) Beck, J. L.; de Jersey, J.; Zerner, B.; Hendrich, M. P.; Debrunner, P. G. *J. Am. Chem. Soc.* **1988**, *110*, 3317.
(16) Borovik, A. S.; Papae3fthymiou, V.; Taylor, L. F.; Anderson, O. P.; Que, L., Jr. *J. Am. Chem. Soc.* **1989**, *111*, 6183.
(17) (a) Holman, T. R.; Andersen, K. A.; Anderson, O. P.; Hendrich, M. P.; Jaurez-Garcia, C.; Münck, E.; Que, L., Jr. *Angew. Chem., Int. Ed. Engl.* **1990**, *29*, 921. (b) Jaurez-Garcia, C.; Hendrich, M. P.; Holman, T. R.; Que, L., Jr.; Münck, E. *J. Am. Chem. Soc.* **1991**, *113*, 518.
(18) Holman, T. R.; Jaurez-Garcia, C.; Hendrich, M. P.; Que, L., Jr.; Münck, E. *J. Am. Chem. Soc.* **1990**, *112*, 7611.
(19) Holman, T. R.; Wang, Z.; Hendrich, M. P.; Que, L., Jr. *Inorg. Chem.* **1995**, *34*, 134.
(20) HBPMP : 2,6-bis[(bis(2-pyridylmethyl)amino)methyl]-4-methylphenol. HBIMP:2,6-bis[bis(1-methylimidazol-2-yl)methyl)amino)methyl]-4-methylphenol.
(21) Strater, N.; Klabunde, T.; Tucker, P.; Witzel, H.; Krebs, B. *Science* **1995**, *268*, 1489.
(22) Aquino, M. S.; Lim, J.-S.; Sykes, A. G. *J. Chem. Soc., Dalton Trans.* **1994**, 429 and references cited therein.
(23) (a) Nanda, K. K.; Mohanta, S.; Ghosh, S.; Mukherjee, M.; Heliwell, M.; Nag, K. *Inorg. Chem.* **1995**, *34*, 2861. (b) Nanda, K. K.; Das, R.; Thompson, L. K.; Venkatsubramanian, K.; Paul, P.; Nag, K. *Inorg. Chem.* **1994**, *33*, 1188. (c) Nanda, K. K.; Thompson, L. K.; Bridson, J. N.; Nag, K. *J. Chem. Soc., Chem. Commun.* **1994**, 1337. (d) Das, R.; Nanda, K. K.; Pal, I.; Baitalik, S.; Nag, K. *Polyhedron* **1994**, *13*, 2639. (e) Das, R.; Nanda, K. K.; Mukherjee, A. K.; Mukherjee, M.; Heliwell, M.; Nag, K. *J. Chem. Soc., Dalton Trans.* **1993**, 2241.
(24) (a) Nanda, K. K.; Das, R.; Thompson, L. K.; Venkatsubramanian, K.; Nag, K. *Inorg. Chem.* **1994**, *33*, 5934. (b) Mohanta, S.; Nanda, K. K.; Thompson, L. K.; Florke, U.; Nag, K. submitted.
(25) (a) Mandal, S. K.; Nag, K. *J. Org. Chem.* **1986**, *51*, 3900. (b) Mandal, S. K.; Thompson, L. K.; Nag, K.; Charland, J.-P.; Gabe, E. J. *Inorg. Chem.* **1987**, *26*, 1391.
(26) Vogel, A. I. *A Text-book of Quantitative Inorganic Analysis*, 3rd ed.; Longmans: England, 1961.
(27) Nanda, K. K.; Dutta, S. K.; Baitalik, S.; Venkatsubramanian, K.; Nag, K. *J. Chem. Soc., Dalton Trans.* **1995**, 1239.

Table 1. Crystallographic Data for $[\{Fe^{III}Co^{III}L(\mu\text{-}OAc)(OAc)\}_2(\mu\text{-}O)](ClO_4)_2\cdot 3H_2O$ (**6**)

formula	$C_{56}H_{80}N_8O_{21}Cl_2Co_2Fe_2\cdot 3H_2O$	Z	8
fw	1555.80	D_{calcd},g cm^{-1}	1.504
cryst size, mm	0.44 × 0.41 × 0.25	λ(Mo Kα), Å	0.71073
cryst syst	orthorhombic	abs coeff, mm^{-1}	1.048
space group	*Ibca*	temp, K	293
a, Å	17.577(4)	F(000)	6480
b, Å	27.282(7)	R^a	0.082
c, Å	28.647(6)	$wR_2{}^b$	0.251
V, Å^3	13.737(6)		

^{a} $R = [\sum||F_o| - |F_c||/\sum|F_o|]$ for $F_o > 4\sigma(F_o)$. ^{b} $wR_2 = [\sum w(F_o^2 - F_c^2)^2/\sum w(F_o^2)^2]^{1/2}$ where $w = 1/[\sigma^2(F_o^2) + (0.0808P)^2 + 57.52P]$ and $P = (F_o^2 + 2F_c^2)/3$.

The electrochemical measurements were performed at room temperature in acetonitrile or dimethylsulfoxide solutions under N_2 using a BAS 100B electrochemical analyzer (Bioanalytical Systems, Inc.). The supporting electrolyte was tetraethylammonium perchlorate (TEAP) (0.1 M) and solutions were ca. 10^{-3} M in complex. Cyclic voltammograms (CV) and differential pulse voltammograms (DPV) were obtained by using a three-electrode assembly (BAS) comprising a platinum disk or glassy carbon disk working electrode, a platinum auxiliary electrode, and a Ag/AgCl reference electrode. The reference electrode was separated from the bulk solution with a salt bridge having a Vycor plug. IR compensation was achieved before each CV was recorded. The ferrocene/ferrocenium couple was used to monitor the reference electrode and was observed at 0.36 V.

Variable-temperature magnetic susceptibilities of powdered samples were measured in the range 4-300 K by using a Faraday-type magnetometer and a Cahn D200 torsion balance. A main solenoid field of 1.5 T and a gradient field of 9.8 T m^{-1} were employed. The instrument was calibrated with $Hg[Co(NCS)_4]$. Pascal's constants were used to calculate the diamagnetic correction.

Crystal Structure Determination of $[\{Fe^{III}Co^{III}L(\mu\text{-}OAc)(OAc)\}_2(\mu\text{-}O)](ClO_4)_2\cdot 3H_2O$ (6). Crystals suitable for structure determination were obtained by diffusing diethyl ether to a solution of **6** in acetonitrile−methanol (1:1) mixture.

Diffraction data were collected on a Siemens R3m/V diffractometer in the $\omega-2\theta$ scan mode at 293 K using graphite-monochromatized Mo Kα radiation. Pertinent crystallographic data are summarized in Table 1. Three standard reflections were periodically monitored and no crystal decay was observed. The intensity data were corrected for Lorentz and polarization effects and semiempirical absorption correction was made from ψ-scans. A total of 7937 reflections were collected in the range $2\theta = 5.5-55.1°$, with $h = 0-22$, $k = 0-35$ and $l = 0-37$, of which 7884 reflections were used for structure determination. The structure was solved by direct and Fourier methods and refined by full-matrix least-squares methods based on F^2 using the programs SHELXTL-PLUS[28] and SHELXL-93.[29] Neutral atom scattering factors were taken from Cromer and Waber.[30] The non-hydrogen atoms were refined anisotropically, while the hydrogen atoms were placed at the geometrically calculated positions with fixed isotropic thermal parameters.

In the asymmetric unit the perchlorate anion was severely disordered, two of the oxygen atoms were refined with a split model. The enclosed water solvent molecules WA2 and WA3 were refined with site occupation factor 0.5, while WA1 lies on a special site. The two carbon sites C(22) and C(23) showed relatively large anisotropic displacement parameters indicating some degree of disorder, but could not be resolved. In the final ΔF map the maximum fluctuations were in the range +0.86 and −0.45 e Å^{-3}.

Results and Discussion

Synthesis. The formation of the heterobimetallic $Fe^{III}M^{II}$ complexes of the binucleating macrocyclic ligand H_2L ideally requires a mononuclear iron(III) precursor complex which, however, is not accessible. On the other hand, the dimeric complex $[Fe_2^{III}(HL)_2(\mu\text{-}OH)_2](ClO_4)_2$, **1**, can be readily obtained by reacting iron(III) perchlorate with H_2L in the presence of either sodium acetate or triethylamine. X-ray crystallographic and spectroscopic studies of **1** have shown[27] that in this compound two macrocyclic FeO_2N_2 cores are linked by two hydroxyl groups and one of the two non-coordinated amine nitrogens in the vacant ligand compartment is protonated. Complex **1** can be deprotonated to the neutral complex $[Fe_2^{III}L_2(\mu\text{-}OH)_2]\cdot 2H_2O$[27] by treating it with 2 equiv of sodium hydroxide.

As shown in Scheme 1 the heterobinuclear complexes $[Fe^{III}M^{II}L(\mu\text{-}OAc)(OAc)(H_2O)](ClO_4)\cdot nH_2O$ (M = Zn, Ni, Co, or Mn) **2**−**5** are obtained by reacting 1 equiv of **1** with 2 equiv of the divalent metal perchlorates and excess of sodium acetate. The cobalt(III) center in **4** can be oxidized with alkaline hydrogen peroxide to produce the heterotetranuclear complex $[\{Fe^{III}Co^{III}L(\mu\text{-}OAc)(OAc)\}_2(\mu\text{-}O)](ClO_4)_2\cdot 3H_2O$, **6**. The yield of **6** is rather poor (ca. 15%) because substantial decomposition

Scheme 1

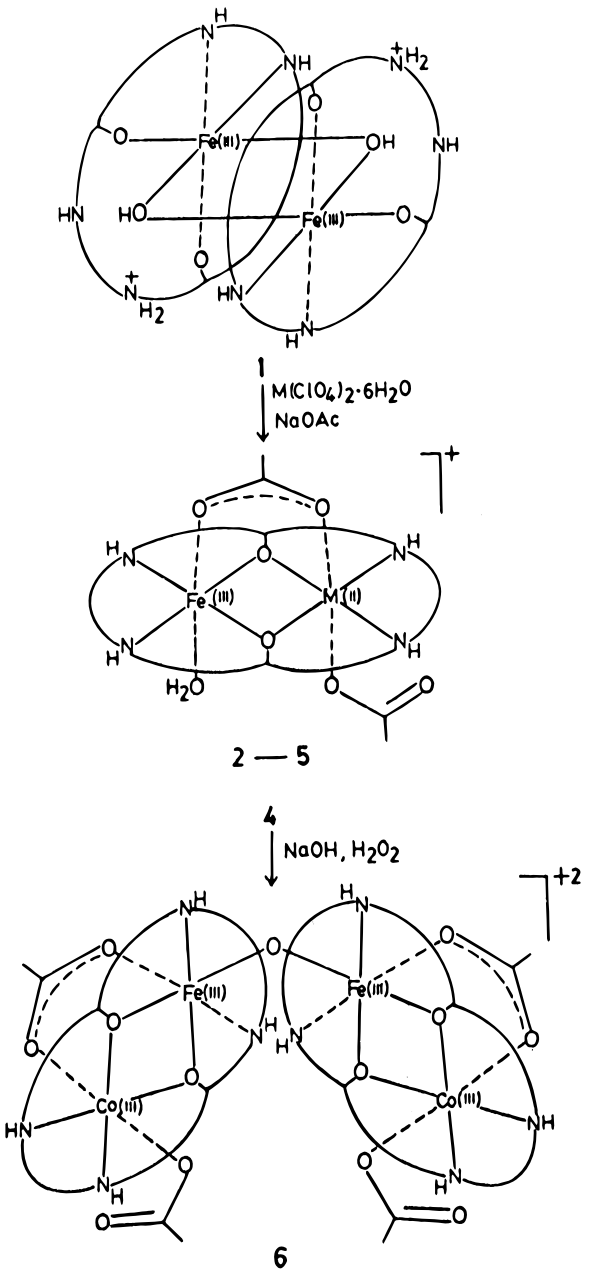

(28) SHELXTL-PLUS; Siemens Crystallographic Research Systems: Madison, WI, 1990.
(29) Sheldrick, G. M. SHELXL-93 A Program for Crystal Structure Refinement. University of Gottingen, Germany, 1993.
(30) Cromer, D. T.; Waber, J. T. *International Tables for X-ray Crystallography*; The Kynoch Press: Birmingham, England, 1974; Vol. IV.

Table 2. Electronic and Infrared Spectral Data for the Complexes

complex	λ_{max}, nm (ϵ, M^{-1} cm^{-1})[a]	IR,[b] cm^{-1}	
		$\nu_{as}(CO_2^-)$	$\nu_s(CO_2^-)$
$[Fe^{III}Zn^{II}L(\mu\text{-OAc})(OAc)(H_2O)](ClO_4)\cdot H_2O$ (**2**)	285 (9300), 320 sh (3500), 505 (2700)	1585 s	1430 m, 1400 m
$[Fe^{III}Ni^{II}L(\mu\text{-OAc})(OAc)(H_2O)](ClO_4)\cdot 2H_2O$ (**3**)	285 (9600), 320 sh (3300), 520 (3100), 1060 (6)	1580 s	1430 m, 1390 m
$[Fe^{III}Co^{II}L(\mu\text{-OAc})(OAc)(H_2O)](ClO_4)\cdot 2H_2O$ (**4**)	285 (10200), 325 sh (3200), 510 (2700), 1000 (27)	1570 s	1420 m, 1380 m
$[Fe^{III}Mn^{II}L(\mu\text{-OAc})(OAc)(H_2O)](ClO_4)\cdot 2H_2O$ (**5**)	285 (10300), 325 sh (3200), 510 (2100)	1580 m, 1545 s	1400 m (br)
$[\{Fe^{III}Co^{III}L(\mu\text{-OAc})(OAc)\}_2(\mu\text{-O})](ClO_4)_2\cdot 3H_2O$ (**6**)	295, 320, 360 (*ca.* 14600), 610 (950)	1550 s	1430 m, 1390 m

[a] In acetonitrile. [b] In KBr.

of the precursor complex occurs due to undesirable side reaction of hydrogen peroxide.

Infrared Spectra. The nature of binding of the acetate ions in **2**−**6** has been ascertained from their IR spectra by considering the difference in energy (Δ) between the asymmetric and symmetric carboxylate stretching frequencies. Commonly, for an unidentate acetate Δ is greater than 150 cm^{-1} and for a bidentate acetate it is less than 100 cm^{-1}, whereas for a bridging acetate Δ is not significantly different from 150 cm^{-1}.[31] For all of the complexes **2**−**5** there are two ranges of Δ values, viz. 145−155 cm^{-1} and 180−190 cm^{-1}, which are clearly indicative of the presence of both bridging and unidentate acetate ions. By contrast, the Δ values for the $[Fe^{III}Co^{III}]_2(\mu\text{-O})$ complex (**6**) (160 and 120 cm^{-1}) do not offer such a clear-cut verdict. It may be noted that the $\nu_{as}(CO_2^-)$ in **6** is shifted to a lower energy (1550 cm^{-1}) relative to those observed in the $Fe^{III}M^{II}$ complexes (ca. 1580 cm^{-1}). This would suggest that the Co^{III}−O (acetate) bonds are stronger compared to the M^{II}−O(acetate) bonds. Indeed, the crystal structure analyses of **3** and **6** have revealed that the Co^{III}−O (acetate) distances in **6** (1.914(6), 1.914(5) Å) are appreciably shorter compared to the Ni^{II}−O(acetate) distances in **3** (2.00, 2.01 Å).

Complex **6** is further characterized by observing a strong band at 845 cm^{-1} due to the Fe−O−Fe asymmetric stretch, while corresponding symmetric stretch is observed as a band of very weak intensity at 420 cm^{-1}. On the basis of the reported correlation[32] between the Fe−O−Fe asymmetric or symmetric stretching frequencies and the oxo-bridge angle in diiron(III) systems the Fe−O−Fe angle in **6** is expected to be 163°, which compares reasonably well with the actual angle 169.5°.

Electronic Spectra. The absorption spectral data for all the complexes are given in Table 2. In the range 250−800 nm complexes **2**−**5** have closely similar spectral features with a sharp band at 285 nm, a shoulder around 325 nm, and a broad band with its peak between 505 and 520 nm. The intense absorption at 285 nm (ϵ = 9300−10300 M^{-1} cm^{-1}) corresponds to the $\pi-\pi^*$ transition of the phenolate anion. The origin of the shoulder at 325 nm is less certain; it may be due to $p\pi-d\sigma^*$ charge transfer of the phenolate oxygen atoms.[33] The band at 510 nm is assigned to phenolate → iron(III) charge transfer (CT) transition. Interestingly, in the hydroxo-bridged diiron(III) complexes $[Fe_2(HL)_2(\mu\text{-OH})_2](ClO_4)_2$ (**1**) and $[Fe_2L_2(\mu\text{-OH})_2]\cdot 2H_2O$ the CT band is blue-shifted to 470 and 465 nm,[27] respectively. The lower charge transfer energies for **2**−**5** relative to that of **1** can be related to the greater Lewis acidity of the iron(III) center in the heterobinuclear complexes.

The absorption spectra of **3** and **4** in the near-IR range exhibit peaks at 1050 and 1000 nm, respectively. In the $Fe^{III}Ni^{II}$ complex the band at 1050 nm can be attributed to $^3A_{2g} \rightarrow {}^3T_{2g}$ transition of high-spin nickel(II) in an octahedral environment,

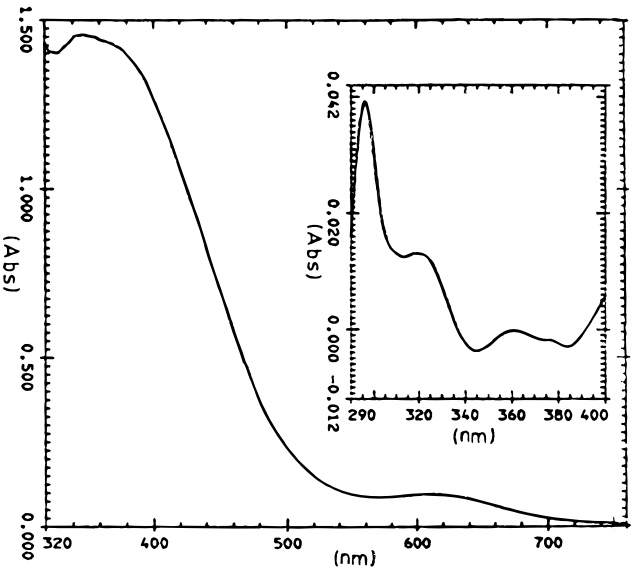

Figure 1. UV−vis spectrum of $[\{Fe^{III}Co^{III}L(\mu\text{-OAc})(OAc)\}_2(\mu\text{-O})](ClO_4)_2\cdot 3H_2O$ (**6**) in acetonitrile solution. Inset shows the derivative absorption spectrum in the UV region.

while the band at 1000 nm in the $Fe^{III}Co^{II}$ complex is due to $^4T_{1g}(F) \rightarrow {}^4T_{2g}$ transition in the six-coordinated cobalt(II) center.

Figure 1 shows the absorption spectrum of $[\{Fe^{III}Co^{III}L(\mu\text{-OAc})(OAc)\}_2(\mu\text{-O})](ClO_4)_2\cdot 3H_2O$ (**6**) in the range 300−800 nm. The electronic spectra of (μ-oxo)diiron(III) complexes are known to exhibit one to three intense absorption features between 300 and 400 nm.[7] These bands were earlier considered to arise due to simultaneous pair excitations,[34] a sequence of combinations of ligand field transitions. However, these bands have been recently interpreted[35] in terms of symmetry related oxo → Fe(III) charge transfer transitions. In the case of $enH_2[\{Fe(HEDTA)\}_2(\mu\text{-O})]\cdot 6H_2O$[34−36] having a Fe−O−Fe angle of 165°,[37] a peak at 285 nm has been assigned to oxo p_z → Fe(III)d_{z^2} CT transition of σ symmetry, while two more absorptions at 315 and 355 nm have been assigned to oxo p_x, p_y → Fe(III)-d_{xz}, d_{yz} CT transitions of π-symmetry. Figure 1 shows that the intense spectral feature in the 280−400 nm region (ϵ = 14 600 M^{-1} cm^{-1}) can be deconvoluted into three peaks at 295, 320, and 360 nm. The close similarity between the spectra of **6** and $enH_2[\{Fe(HEDTA)\}_2(\mu\text{-O})]\cdot 6H_2O$ is in keeping with their Fe−O−Fe angles of 169.5(4) and 165°, respectively. Finally, the absorption maximum observed at 610 nm (ϵ = 950 M^{-1} cm^{-1}) in **6** is assignable to $^1A_{1g} \rightarrow {}^1T_{1g}$ transition of the cobalt(III) center.

(31) Nakamoto, K. *Infrared and Raman Spectra of Inorganic and Coordination Compounds*, 3rd ed.; John Wiley: New York, 1978; p 232.
(32) Sanders-Loehr, J.; Wheeler, W. D.; Shiemke, A. K.; Averill, B. A.; Loehr, T. M. *J. Am. Chem. Soc.* **1989**, *111*, 8084.
(33) Gaber, B. P.; Miskowski, V.; Spiro, T. G. *J. Am. Chem. Soc.* **1974**, *96*, 6868.
(34) Schugar, H. J.; Rossman, G. R.; Baraclough, C. J.; Gray, H. B. *J. Am. Chem. Soc.* **1972**, *94*, 2683.
(35) Reem, R. C.; McCormick, J. M.; Richardson, D. E.; Devlin, F. J.; Stephens, P. J.; Musselman, R. L.; Solomon, E. I. *J. Am. Chem. Soc.* **1989**, *111*, 4688.
(36) EDTA: *N*,*N*,*N*′,*N*′-ethylenediaminetetraacetate(4−). en: ethylenediamine.
(37) Lippard, S. J.; Schugar, H. J.; Walling, C. *Inorg. Chem.* **1967**, *6*, 127.

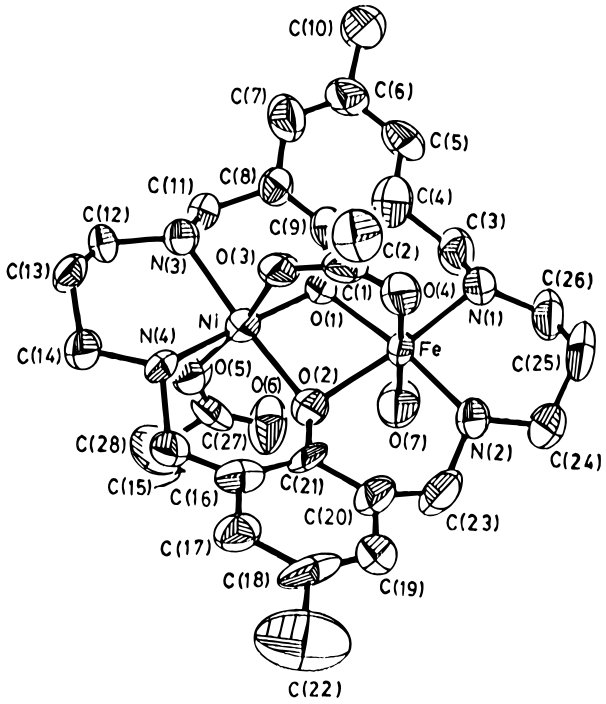

Figure 2. Perspective view of $[Fe^{III}Ni^{II}L(\mu\text{-OAc})(OAc)(H_2O)]^{2+}$ cation in **3**.

Structure of $[Fe^{III}Ni^{II}L(\mu\text{-OAc})(OAc)(H_2O)](ClO_4)\cdot 2H_2O$ (3). The analytical and spectroscopic data of the heterobinuclear complexes **2**−**5** indicate that they have closely related structures. However, since it was still not obvious whether the monodentate acetate anion is bound to the iron(III) or to the bivalent metal ion, the structural analysis of **3** was undertaken.[38] Unfortunately, refinement of the structure was hampered ($R = 0.123$) due to rather inferior quality of diffraction data and severe disordering of the perchlorate anions. Nonetheless, the structural analysis has elucidated the geometric features and connectivities in the complex molecule. The structure of the discrete cation $[FeNiL(\mu\text{-OAc})(OAc)(H_2O)]^+$ (Figure 2) shows that the two metal centers are bridged by the two phenolate oxygens as well as by an acetate. Both the metal centers are six-coordinated with irregular octahedral geometry and have N_2O_2 equatorial donors provided by the macrocyclic ligand. The remaining apical position of the iron(III) center is occupied by a water molecule, while that of the nickel(II) by an acetate oxygen. The relevant metal−donor distances[39] are generally in accord with the high-spin configurations of both Fe(III) and Ni(III). The nonbonded Fe···Ni distance is 3.03Å.

Structure of $[\{Fe^{III}Co^{III}L(\mu\text{-OAc})(OAc)\}_2(\mu\text{-O})](ClO_4)_2\cdot 3H_2O$ (6). The ORTEP representation of the complex cation in **6** along with the atom labels are shown in Figure 3. Atomic coordinates and selected bond distances and angles are given in Tables 3 and 4, respectively. The structure of the cation in **6** comprises two identical heterobinuclear $Co^{III}Fe^{III}$ cores joined by a Fe−O−Fe linkage. The cation is not centrosymmetric (the space group is however), but does have a 2-fold rotational symmetry. The iron and cobalt centers in the asymmetric unit, similar to that in **3**, are triply bridged by two phenoxides and an acetate ion. The coordination sphere CoO_4N_2 is completed by two equatorial amine nitrogen donors of the ligand and an axial acetate anion. The iron(III) center is also six-coordinated and its remaining coordination sites are occupied by the other two nitrogen atoms of the macrocycle. The structure of **6**, in retrospect, verifies that its precursor **4** is isostructural with **3**.

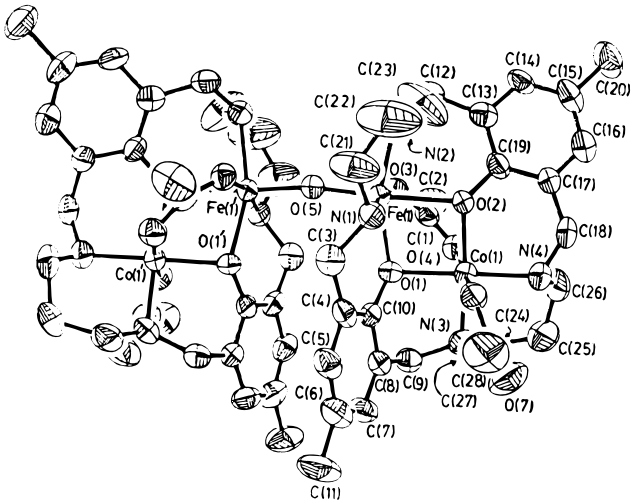

Figure 3. ORTEP representation of the structure of $[\{Co^{III}Fe^{III}L(\mu\text{-OAc})(OAc)\}_2(\mu\text{-O})]^{2+}$ cation in **6**.

The structural features of the cobalt(III) center indicate a regular octahedral geometry and the relevent bond distances are consistent with its spin-paired configuration. By contrast, the iron(III) center has a highly distorted octahedral geometry. The two $Fe-O_{phenolate}$ distances (1.990(5) and 2.140(5) Å) are dissimilar, as are the bond lengths of $Fe-O_{acetate}$ (2.084(5) Å) and $Fe-O_{oxo}$ (1.7895(12) Å). It may be noted that the Fe−N distances (average 2.15(1) Å) of high-spin iron(III) are considerably longer compared to the low-spin $Co^{III}-N$ distances (average 1.96(1) Å). The oxo−iron distance (1.7895(12) Å) and Fe−O−Fe angle (169.5(4)°) are well within the ranges 1.71−1.81 Å and 135−180° reported for singly bridged (μ-oxo)diiron(III) systems.[7] A pronounced trans influence of the $Fe-O_{oxo}$ groups is manifestated in lengthening of the Fe−O(2) bond (2.140(5) Å) relative to the Fe−O(1) bond (1.990(5) Å). In the heterobinuclear unit the nonbonding Fe···Co distance (3.029(1) Å) is very similar to that of Fe···Ni distance (3.03 Å) in **3**. On the other hand, the Fe···Fe distance (3.564(1) Å) again is in consonance with the range 3.39−3.56 Å reported for μ-oxo-monobridged complexes.[7] As an aside, we note that the Fe···Fe distance in the dihydroxo-bridged complex **1** is 3.085(3) Å.[27]

In the heterobinuclear unit the cobalt atom lies exactly on the mean plane of O(1), O(2), N(3), N(4) atoms, while the iron atom is displaced from the mean plane of N(1), N(2), O(1), O(3) atoms by 0.256 Å. The dihedral angle between these two planes is 78.2°. The carboxylate bridge in the $Fe^{III}Co^{III}$ unit imposes a convex motif to the macrocycle when viewed down this bridge, as a result of which the two phenyl rings are inclined to each other by 124.1°.

Electrochemistry. Cyclic voltammetric and differential pulse voltammetric measurements have been carried out for complexes **2**−**6**, and the results for **2**−**5** are summarized in Table 5. In the potential range 0 to −1 V the electrochemical behavior of all the heterobimetallic complexes in dimethyl sulfoxide solution are quite similar, and they exhibit a quasi-reversible $Fe^{III}M^{II}/Fe^{II}M^{II}$ couple having Nernstian characteristics; viz. $E_{1/2}$ remains constant as a function of scan rate (υ) and the peak current ratio (I_{pc}/I_{pa}) is close to unity. It may be seen from Table 5 that the

(38) $[C_{28}H_{42}N_4O_7NiFe](ClO_4)\cdot 2H_2O$; tetragonal, space group $P4_32_12_1$, $a = 14.284(2)$ Å, $c = 38.604(12)$ Å, $Z = 8$, $V = 7877(3)$ Å^3. X-ray data were collected and processed in the same way as described for **6**. Out of 9930 reflections measured, 9063 were used for structure analysis. $I > 2\sigma(I)$: $R = 0.123$, $wR_2 = 0.3054$.

(39) Selected bond lengths (Å): Ni−O(1) = 2.03, Ni−O(2) = 2.03, Ni−O(3) = 2.00, Ni−O(5) = 2.01, Ni−N(3) = 2.13, Ni−N(4) = 2.14, Fe−O(1) = 2.14, Fe−O(2) = 2.13, Fe−O(4) = 2.04, Fe−O(7) = 2.06, Fe−N(1) = 2.09, Fe−N(2) = 2.06.

Table 3. Atomic Coordinates[a] ($\times 10^4$) and Equivalent Isotropic Thermal Parameters U_{eq}[b] ($Å^2 \times 10^3$) of the Non-Hydrogen atoms for **6**

atom	*x*	*y*	*z*	U_{eq}
Co(1)	4335(1)	1066(1)	1373(1)	45(1)
Fe(1)	4915(1)	1849(1)	714(1)	39(1)
O(1)	4699(3)	1739(2)	1388(2)	41(1)
O(2)	4727(3)	1075(2)	735(2)	42(1)
O(3)	3737(3)	1860(2)	630(2)	45(1)
O(4)	3371(3)	1280(2)	1138(2)	53(2)
O(5)	5000	2500	656(2)	45(2)
O(6)	5339(3)	871(2)	1554(2)	52(1)
O(7)	5133(5)	541(3)	2250(3)	106(3)
N(1)	6092(4)	1735(2)	906(2)	49(2)
N(2)	5153(4)	1686(3)	0(2)	64(2)
N(3)	3895(4)	1123(3)	2003(2)	58(2)
N(4)	4058(5)	375(2)	1363(2)	65(2)
C(1)	3239(5)	1608(3)	835(3)	51(2)
C(2)	2424(5)	1700(4)	721(4)	89(3)
C(3)	6306(4)	2069(3)	1298(3)	52(2)
C(4)	5888(5)	1983(3)	1749(3)	49(2)
C(5)	6280(5)	2053(3)	2170(3)	56(2)
C(6)	5935(6)	2006(4)	2603(3)	65(3)
C(7)	5180(6)	1875(3)	2614(3)	62(2)
C(8)	4777(5)	1794(3)	2205(3)	49(2)
C(9)	3963(5)	1627(3)	2200(3)	57(2)
C(10)	5127(4)	1849(3)	1771(2)	42(2)
C(11)	6378(7)	2071(5)	3051(3)	97(4)
C(12)	4482(5)	1475(3)	−236(3)	61(2)
C(13)	4275(4)	967(3)	−64(3)	48(2)
C(14)	3955(5)	649(3)	−391(3)	58(2)
C(15)	3709(5)	185(3)	−287(3)	65(3)
C(16)	3833(5)	25(3)	169(3)	62(2)
C(17)	4170(5)	315(3)	503(3)	53(2)
C(18)	4402(6)	113(3)	963(3)	66(3)
C(19)	4386(5)	795(3)	392(3)	47(2)
C(20)	3341(7)	−146(4)	−651(4)	91(4)
C(21)	6623(6)	1831(5)	521(4)	99(4)
C(22)	6568(7)	1551(7)	115(5)	150(7)
C(23)	5848(6)	1353(5)	−51(5)	122(5)
C(24)	3099(6)	940(4)	2053(3)	79(3)
C(25)	3020(7)	396(4)	1928(4)	104(4)
C(26)	3247(6)	269(4)	1438(3)	84(3)
C(27)	5563(7)	683(4)	1940(4)	71(3)
C(28)	6410(7)	627(4)	1988(4)	106(4)
Cl(1)	8474(2)	1354(2)	1368(1)	126(2)
O(111)	8575(16)	973(10)	1814(6)	182(10)[a]
O(112)	8508(13)	1894(7)	1138(9)	157(9)[a]
O(12)	9213(7)	1297(6)	1342(5)	203(6)
O(131)	8219(14)	1706(10)	1628(9)	135(8)[a]
O(132)	7985(13)	1451(10)	1749(8)	133(8)[a]
O(14)	8088(6)	1089(4)	1047(3)	138(4)
WA1	5000	2500	−823(7)	201(7)[a]
WA2	4823(18)	−427(11)	1861(10)	210(12)[a]
WA3	5408(12)	508(6)	3250(6)	113(6)[a]

[a] Site occupancy = 0.50. [b] U_{eq} is defined as one-third of the trace of the orthogonalized U_{ij} tensor.

variation of the M^{II} ions has marginal effect on $E_{1/2}$ values (−0.44 to −0.48 V vs Ag/AgCl). The bivalent metal center in complexes **3**−**5** can be electrochemically oxidized. The CV of **4** in acetonitrile recorded in the potential window 0 to +1 V showed that while the oxidation of $Fe^{III}Co^{II}$ to $Fe^{III}Co^{III}$ occurs quasireversibly with $E_{1/2}$ = 0.74 V and ΔE_p = 220 mV (υ = 100 mV/s); both **3** and **5** get irreversibly oxidized at 0.85 V.

The CV and DPV of **6** in dimethyl sulfoxide solution showed a few interesting features. When a freshly polished glassy carbon electrode is used, in the negative potential regime a quasireversible redox couple is followed by an irreversible electron transfer reaction due to $Fe^{III}Co^{III}/Fe^{III}Co^{II}$ ($E_{1/2}$ = −0.15 V) and $Fe^{III}Co^{II}/Fe^{II}Co^{II}$ (E_p = −0.84 V). The nature of the voltammogram at the more negative potential indicates that following the electron transfer a chemical reaction takes place. Repetition

Table 4. Selected Bond Distances (Å) and Angles (deg) for $[\{Fe^{III}Co^{III}L(\mu\text{-OAc})(OAc)\}_2(\mu\text{-O})](ClO_4)_2\cdot 3H_2O$ (**6**)

Co(1)−O(1)	1.947(5)	Fe(1)−O(1)	1.990(5)
Co(1)−O(2)	1.955(5)	Fe(1)−O(2)	2.140(5)
Co(1)−N(3)	1.971(7)	Fe(1)−N(1)	2.163(6)
Co(1)−N(4)	1.946(7)	Fe(1)−N(2)	2.135(7)
Co(1)−O(4)	1.914(6)	Fe(1)−O(3)	2.084(5)
Co(1)−O(6)	1.914(5)	Fe(1)−O(5)	1.7895(12)
Co(1)···Fe(1)	3.029(1)	Fe(1)···Fe(1a)	3.564(1)
N(4)−Co(1)−N(3)	89.5(3)	O(1)−Fe(1)−O(2)	78.2(2)
O(2)−Co(1)−O(1)	83.8(2)	N(1)−Fe(1)−N(2)	91.5(3)
N(4)−Co(1)−O(2)	95.0(3)	O(3)−Fe(1)−O(2)	82.2(2)
N(3)−Co(1)−O(1)	92.0(2)	O(1)−Fe(1)−O(3)	85.6(2)
O(4)−Co(1)−N(4)	94.0(3)	O(1)−Fe(1)−N(1)	85.1(2)
O(4)−Co(1)−O(2)	88.8(2)	O(5)−Fe(1)−O(1)	104.7(2)
O(4)−Co(1)−N(3)	87.2(3)	O(5)−Fe(1)−O(3)	93.3(2)
O(4)−Co(1)−O(1)	90.6(2)	O(5)−Fe(1)−N(2)	95.9(3)
O(6)−Co(1)−O(1)	87.3(2)	O(5)−Fe(1)−N(1)	95.0(2)
O(6)−Co(1)−O(2)	86.1(2)	O(2)−Fe(1)−N(1)	89.9(2)
O(6)−Co(1)−N(3)	97.8(3)	O(3)−Fe(1)−N(2)	95.1(3)
O(6)−Co(1)−N(4)	88.0(3)	O(1)−Fe(1)−N(2)	159.3(2)
O(6)−Co(1)−O(4)	174.6(2)	O(5)−Fe(1)−O(2)	174.5(2)
O(2)−Co(1)−N(3)	174.1(3)	O(3)−Fe(1)−N(1)	168.9(2)
O(1)−Co(1)−N(4)	175.3(3)	Fe(1)−O(5)−Fe(1a)[a]	169.5(4)
Co(1)−O(1)−Fe(1)	100.6(2)	Co(1)−O(2)−Fe(1)	95.3(2)

[a] Symmetry transformation used to generate equivalent atom: $-x+1, -y+{}^1/_2, z+1-1$.

Table 5. Electrochemical Data[a] for Complexes **2**−**5**

	$E_{1/2}$(reduction)[b] $M^{II}Fe^{III}/M^{II}Fe^{II}$			$E_{1/2}$(oxidation)[c] $M^{II}Fe^{III}/M^{III}Fe^{III}$		
complex	CV[d]	DPV[e]	ΔE_p[f]	CV[d]	DPV[e]	ΔE_p[f]
2	−0.435	−0.440	125			
3	−0.475	−0.480	100	0.85[g]	0.840	
4	−0.458	−0.460	95	0.742	0.737	220
5	−0.438	−0.435	150	0.85[g]	0.845	

[a] All potentials are referenced to Ag/AgCl electrode. [b] In dimethyl sulfoxide solution. [c] In acetonitrile solution. [d] At a scan rate of 100 mV s^{-1}. [e] Potential corrected for modulation amplitude (50 mV) at a scan rate of 20 mV s^{-1}. [f] Separation between $E_{p,c}$ and $E_{p,a}$ in CV expressed in mV. [g] Irreversible oxidation.

of scanning between 0 and −1 V leads to the emergence of a new redox couple. The characteristic features of this new redox couple, $E_{1/2}$ = −0.47 V and ΔE_p = 100 mV (υ = 100 mV/s), are identical to that of the $Fe^{III}Co^{II}/Fe^{II}Co^{II}$ couple observed in **4**. The electrochemical generation of the $Fe^{II}Co^{II}$ species from the $[Fe^{III}Co^{III}]_2(\mu\text{-O})$ complex may be rationalized by considering the following reactions:

$$[\{Fe^{III}Co^{III}L(\mu\text{-OAc})(OAc)\}_2(\mu\text{-O})]^{2+} + 2e^- \underset{}{\overset{-0.15\ V}{\rightleftharpoons}} [\{Fe^{III}Co^{II}L(\mu\text{-OAc})(OAc)\}_2(\mu\text{-O})]^0 \quad (1)$$

$$[\{Fe^{III}Co^{II}L(\mu\text{-OAc})(OAc)\}_2(\mu\text{-O})]^0 + 2e^- + 3H_2O \xrightarrow{-0.84\ V} 2[Fe^{II}Co^{II}L(\mu\text{-OAc})(OAc)(H_2O)]^0 + 2OH^- \quad (2)$$

$$[Fe^{II}Co^{II}L(\mu\text{-OAc})(OAc)(H_2O)] \underset{}{\overset{-0.47\ V}{\rightleftharpoons}} [Fe^{III}Co^{II}L(\mu\text{-OAc})(OAc)(H_2O)]^+ + e^- \quad (3)$$

NMR Spectra. The ^1H NMR spectroscopic behavior of the oxo-bridged $[Fe^{III}Co^{III}]_2(\mu\text{-O})$ complex (**6**) has been studied at room temperature in CD_3CN and CD_3NO_2 solutions. The spectral features of the compound in CD_3CN (shown in Figure 4), which remain unaltered in CD_3NO_2, indicate that the symmetric structure of the complex cation is retained in solution. This fact, along with the strong antiferromagnetic exchange

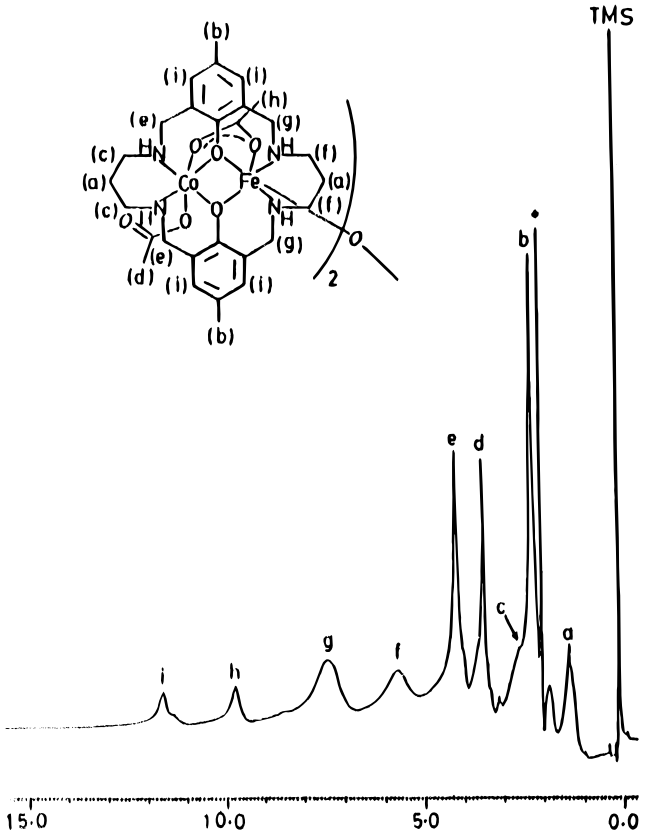

Figure 4. ^{1}H NMR spectrum of **6** in CD_3CN. Inset shows assignments of resonances.

coupling between the two iron(III) centers ($S = {}^5/_2$) in the Fe−O−Fe moiety and the presence of a spin-paired ($S = 0$) cobalt(III) center in the heterobimetallic unit have rendered the spectrum rather simple. In fact, the chemical shifts occur in a remarkably narrow range of 1−12 ppm for a paramagnetic compound. The spectral assignments made (shown in the inset of Figure 4) are based on the known chemical shift data of the macrocyclic ligand,[25] proximities of different protons from the paramagnetic metal center, and integration of the peaks.

The three sharp signals observed at 2.25, 3.55, and 4.30 ppm can be attributed to *p*-CH_3 (b), the cobalt-bound acetate (d), and cobalt adjoining $ArCH_2$ (e) proton resonances, respectively. The $CH_2CH_2CH_2$ (a) protons experience maximum upfield shift (1.35 ppm), while the resonances due to the $CH_2CH_2CH_2$ (c) protons near the cobalt atom are not resolved (ca. 2.7 ppm) and they partly overlap with the *p*-CH_3 signal. The two most broad signals at 5.8 and 7.5 ppm are assignable to the protons of $CH_2CH_2CH_2$ (f) and $ArCH_2$ (g) in the vicinity of the iron center. Finally, the two relatively less broadened peaks appearing at 9.8 and 11.7 ppm can be assigned to the bridged acetate (h) and meta protons (i), respectively. Thus, except for the NH protons all other moities are observed. In contrast to **6**, the protons in the $Fe^{III}Zn^{II}$ complex (**2**) undergo pronounced isotropic shifts and are observed in the range −5 to +80 ppm. However, the very broad nature of these resonances have failed to reveal useful structural information for **2**.

Magnetic Properties. The variable-temperature (4−300 K) magnetic susceptibility data were collected for powdered samples of **1** and **3**−**6**. The variations of molar magnetic susceptibility (χ_M) and magnetic moment per molecule (μ_{eff}) with temperature for some of these compounds are illustrated in Figures 5−7. Analysis of the susceptibility data has been carried out using the isotropic Heisenberg−Dirac−van Vleck model with the spin Hamiltonian $H = -2JS_1 \cdot S_2$. The theoretical

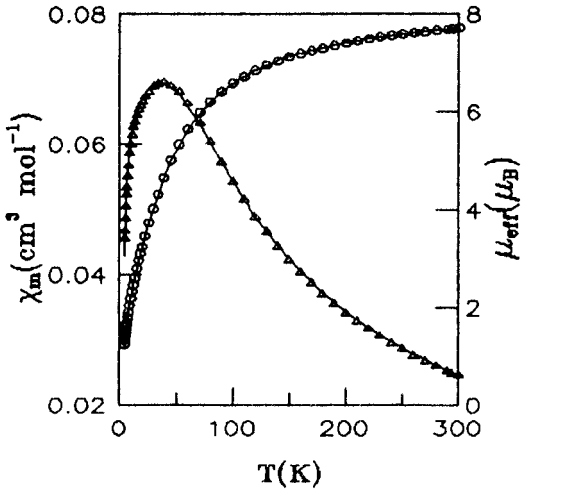

Figure 5. Molar magnetic susceptibility data (△) and effective magnetic moment (○) vs temperature for **1**. The solid lines result from a least-squares fit to the theoretical expression.

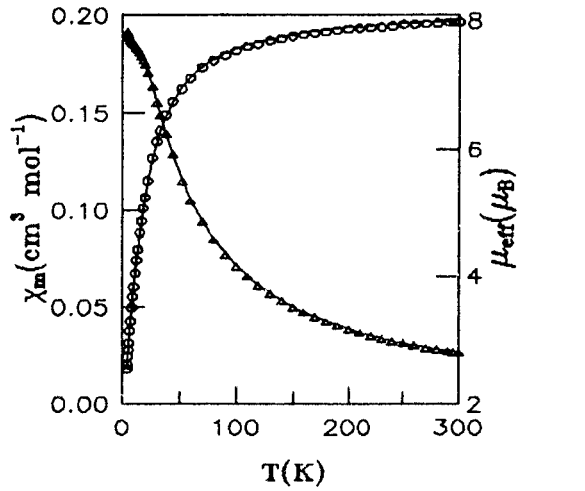

Figure 6. Molar magnetic susceptibility data (△) and effective magnetic moment (○) vs temperature for **5**. The solid lines result from a least-squares fit to the theoretical expression.

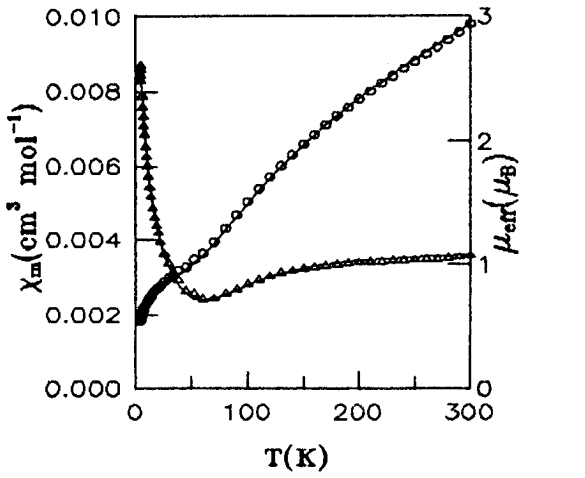

Figure 7. Molar magnetic susceptibility data (△) and effective magnetic moment (○) vs temperature for **6**. The solid lines result from a least-squares fit to the theoretical expression.

expressions for χ_M for different systems, as given elsewhere,[40] have been modified to include the fraction *p* of a mononuclear paramagnetic impurity present, whose contribution is averaged

(40) O'Connor, C. J. *Prog. Inorg. Chem.* **1979**, *29*, 204.

Table 6. Magnetic Data for the Complexes

complex[a]	J, cm^{-1}	g	p,%	Θ, K	10^2R[b]
$[Fe^{III}_2(HL)_2(\mu\text{-}OH)_2](ClO_4)_2$ (**1**)	−4.5(1)	1.98(1)	2.6	−1.2	0.95
$[Fe^{III}Ni^{II}L(\mu\text{-}OAc)(OAc)(H_2O)](ClO_4)\cdot 2H_2O$ (**3**)	1.7(1)	2.12(1)	0	−0.1	1.92
$[Fe^{III}Co^{II}L(\mu\text{-}OAc)(OAc)(H_2O)](ClO_4)\cdot 2H_2O$ (**4**)	4.2(2)	2.27(2)	0.2	0	6.85
$[Fe^{III}Mn^{II}L(\mu\text{-}OAc)(OAc)(H_2O)](ClO_4)\cdot 2H_2O$ (**5**)	−1.85(5)	1.97(1)	4.0	0	0.30
$[\{Fe^{III}Co^{III}L(\mu\text{-}OAc)(OAc)\}_2(\mu\text{-}O)](ClO_4)_2\cdot 3H_2O$ (**6**)	−100(1)	2.00(2)	2.4	−8.4	1.35

[a] TIP × 10^6 (cm^3 mol^{-1}): **1**, 160; **3**, 180; **4**, 80; **5**, 80; **6**, 500. [b] $R = [\sum(\chi_{obs} - \chi_{calc})^2/\sum(\chi_{obs})^2]^{1/2}$.

between the two spin states in the heterobimetallic complexes, and the Weiss term Θ to account for any intermolecular interactions between entities containing either a unique magnetic center or dinuclear units. Further, the following values of temperature-independent paramagnetism (TIP × 10^6 cm^3 mol^{-1}) have been used: iron(III), 80; cobalt(III), 170; nickel(II), 100; manganese(II), 0; cobalt(II), 0. Nonlinear least-squares fittings of the theoretical expressions to the experimental data have been made by varying J, g, p, and Θ and minimizing the residual $R = [\sum(\chi_{obs} - \chi_{calc})^2/\sum(\chi_{obs})^2]^{1/2}$. Table 6 summarizes the spin exchange integrals along with other relevant parameters.

As shown in Figure 5 for the hydroxo-bridged diiron(III) complex **1**, χ_M passes through a maximum at 35K with lowering of the temperature and the moment per iron(III) decreases from 5.46 μ_B (300.2 K) to 0.89 μ_B (4.3 K). Satisfactory simulation of the experimental data gives $J = -4.5$ cm^{-1} and $g = 1.98$.

The cryomagnetic behavior of the $Fe^{III}Mn^{II}$ complex (**5**) also indicates a weak antiferromagnetic exchange interaction. Figure 6 shows that with lowering of the temperature μ_{eff} slowly decreases from 7.98 μ_B (299.9 K) to 7.10 μ_B (60.0 K) and then more rapidly reaches a value of 2.57 μ_B at 4.3 K. Least-squares fitting the data for **5** gives $J = -1.8$ cm^{-1} and $g = 1.97$. It may be noted that the quality of fit is excellent, albeit the zero-field parameters for the manganese(II) have not been considered. This indicates that the effect of the zero-field splitting in this case is nominal.

The χ_M vs T and μ_{eff} vs T plots of the $[Fe^{III}Co^{III}]_2(\mu\text{-O})$ complex (**6**), as shown in Figure 7, are typical of oxo-bridged diiron(III) complexes exhibiting fairly strong antiferromagnetic exchange interaction. The best fit parameters obtained in this case are $J = -100$ cm^{-1} and $g = 2.00$, with a fairly large contribution due to $\Theta = -8.4$ K. To account for this large Θ contribution the possibility of intermolecular interactions involving hydrogen bonding/or aromatic stacking was considered. The crystal packing of **6**, however, did not reveal any relevant intermolecular hydrogen bonding pattern. The aromatic part C(13)−C(16) is indeed parallel to a second molecule, but the midpoints of these rings are 4.27 Å apart. If Θ is ignored, the quality of fit deteriorates, albeit the value of J remains practically unchanged.

The cryomagnetic behavior of the $Fe^{III}Ni^{II}$ complex **3** showed that the moment of the complex monotonically increases from 6.95 to 8.31 μ_B as the temperature decreases from 299.0 to 7.4 K. However, further cooling leads to a decrease of the moment and a value of 8.00 μ_B is reached at 4.3 K. The observed behavior is consistent with ferromagnetic coupling between the Fe^{III} ($S_1 = {}^5/_2$) and Ni^{II} ($S_2 = 1$) centers, for which a $S = {}^7/_2$ ground state is expected to have a moment of 8.43 μ_B with $g = 2.125$. Fitting of the experimental data to the theoretical expression gave $J = 1.7$ cm^{-1} and $g = 2.125$. The anomaly observed below 7.4 K appears to be due to the zero-field splitting effect of the nickel(II).

The magnetic property of the $Fe^{III}Co^{II}$ complex (**4**) is similar to that of **3**. In the temperature range 299.9−9.8 K the moment steadily increases from 8.27 to 10.16 μ_B, a value which corresponds to $S_T = 4$ with g = 2.27 resulting from the ferromagnetic coupling between the Fe^{III} ($S_1 = {}^5/_2$) and Co^{II} ($S = {}^3/_2$) centers. Again similar to **3**, the μ_{eff} of **4** begins to decrease below 9.8 K and attains a value of 9.45 μ_B at 4.3 K. The experimental data could be reasonably fitted with $J = 4.2$ cm^{-1} and $g = 2.27$.

The magnetic data of the compounds summarized in Table 6 reveal that in contrast to the weak antiferromagnetic exchange in the d^5−d^5 systems (**1** and **5**), weak ferromagnetic coupling occurs for the d^5−d^8 (**3**) and d^5−d^7 (**4**) systems. The magnetic property of **6** with $J = -100$ cm^{-1} is consistent with the reported behavior of oxo-bridged diiron(III) complexes, $-J$ values for the vast majority of which fall into the 80−120 cm^{-1} range.[7] The magnetostructural data available for a few dihydroxo-bridged diiron(III) complexes disclose[7] that $-J$ values fall in the range 7−12 cm^{-1} when Fe···Fe distance lies between 3.08 and 3.15 Å and the Fe−OH−Fe bridge angle varies from 102.8 to 105.3°. In comparison with these values, for **1** $J = -4.5$ cm^{-1}, the Fe···Fe distance is 3.085°, and the bridge angle is 100.7(4)°.[27]

Magnetic properties of very few heterobimetallic $Fe^{III}Mn^{II}$ complexes have been studied so far. The triply bridged Fe^{III}-Mn^{II} complexes derived from HBPMP[19,20] and HBIMP,[20,41] both having the μ-phenoxo−bis-(μ-carboxylate) core, have been reported to exhibit antiferromagnetic exchange coupling with J values of −11.5 cm^{-1} (HBPMP)[19] and −7.7 cm^{-1} (HBIMP).[41] Complex **5**, which is also triply bridged but has the μ-carboxylate−bis(μ-phenoxo) core, exhibits weaker antiferromagnetic exchange ($J = -1.8$ cm^{-1}). The difference in the behavior of these two cores may be qualitatively understood in terms of the Goodenough−Kanamori rules[42,43] of interactions between pairs of magnetic orbitals. In the case of d^5−d^5 systems an overall antiferromagnetic effect is expected,[44,45] although the possibility of weak ferromagnetic interaction cannot be entirely ruled out. Further, antiferromagnetic interaction is expected to increase with the expansion of bridge angle.[45] Considering that **5** is isostructural with **3**, the Fe−O(phenoxo)−Mn angles in **5** can be reasonably expected to be more acute than their counterparts in the HBPMP or HBIMP derived compounds.

The difference in the cryomagnetic behavior of the $Fe^{III}Ni^{II}$ complexes viz. **3** and the one derived from HBPMP[18] are even more striking. In **3** the overall exchange interaction is ferromagnetic ($J = 1.7$ cm^{-1}) with an $S = {}^7/_2$ ground state, while in the $Fe^{III}Ni^{II}$−BPMP complex the two metal ions are antiferromagnetically coupled ($J = -11.5$ cm^{-1}) with an $S = {}^3/_2$ ground state. This difference can be rationalized again in the framework of orbital symmetry properties. For d^5−d^8 ions in octahedral environment it has been predicted[45] that when the bridge angle is close to 90° the interaction will be ferromagnetic; on the other hand, for a larger bridge angle the interaction will be antifer-

(41) Buchanan, R. M.; Mashuta, M. S.; Richardson, J. F.; Oberausen, K. J.; Hendrickson, D. N.; Webb, R. J.; Nanny, M. A. *Inorg. Chem.* **1990**, *29*, 1299.
(42) Goodenough, J. B. *J. Phys. Chem. Solids* **1958**, *6*, 287.
(43) Kanamori, J. *J. Phys. Chem. Solids* **1959**, *10*, 87.
(44) Ginsberg, A. P. *Inorg. Chim. Acta Rev.* **1971**, *5*, 45.
(45) Kahn, O. *Molecular Magnetism*; VCH Publishers: New York, 1993.

romagnetic. In agreement with these expectations, we note that the Fe−O(phenoxo)−Ni bridge angles in **3** and the PMBP complex are 92.8(4) and 116.2(2)°,[18] respectively.

Along the same line of reasoning one would expect **4** to behave ferromagnetically, which, indeed has the ground state $S = 4$ and $J = 4.2$ cm^{-1}. Moreover, in this case the t_{2g} orbitals of the cobalt(II) ion are not completely filled, and hence there are more pathways for ferromagnetic coupling. Thus, a relatively stronger ferromagnetic interaction observed in **4** relative to that in **3** is quite in order.

Acknowledgment. K.N. thanks the Department of Science and Technology, Government of India, for financial support of this research.

Supporting Information Available: Tables of analytical results for **2**−**6** (Table S1), thermal parameters (Table S2), hydrogen atom coordinates (Table S3), and complete bond lengths and angles (Table S4) for **6** (5 pages). Ordering information is given on any current masthead page.

IC9508334